Background to $K_L^0 \rightarrow \pi^0 ee$ from $K_L^0 \rightarrow \gamma\gamma ee$

H. B. Greenlee*

Physics Department, Yale University, New Haven, Connecticut 06511

The background to $K_L^0 \rightarrow \pi^0 ee$ from $K_L^0 \rightarrow \gamma\gamma ee$ ($K_L^0 \rightarrow \gamma ee$ with a hard internal bremsstrahlung) is calculated. The consequences for future $K_L^0 \rightarrow \pi^0 ee$ experiments are discussed. It is argued that this background is a serious problem at the sensitivity needed to detect $K_L^0 \rightarrow \pi^0 ee$ at the level predicted by the standard model.

I. INTRODUCTION

The decay mode $K_L^0 \rightarrow \pi^0 ee$ has recently attracted considerable theoretical and experimental interest as a possible probe of CP violation in the standard model. The standard model predicts[1,2] that $K_L^0 \rightarrow \pi^0 ee$ should occur at a branching ratio of order 10^{-11}. Several experiments have searched for $K_L^0 \rightarrow \pi^0 ee$, so far with negative results.[3,4] The best upper limit obtained for the branching ratio of $K_L^0 \rightarrow \pi^0 ee$ is 5.5×10^{-9} (90% C.L.),[4] which is still about two orders of magnitude above the standard-model prediction. More sensitive experiments are planned[5] with sensitivities of order 10^{-11}.

Experiments sensitive to $K_L^0 \rightarrow \pi^0 ee$ at a branching ratio of 10^{-11} will face several formidable backgrounds. One of the worst backgrounds will be from the decay mode $K_L^0 \rightarrow \gamma\gamma ee$, that is, from $K_L^0 \rightarrow \gamma ee$ with a hard internal bremsstrahlung. This process is a fundamental physics background to $K_L^0 \rightarrow \pi^0 ee$ which will be difficult to reduce below a certain level.

The only kinematic difference between $K_L^0 \rightarrow \gamma\gamma ee$ and $K_L^0 \rightarrow \pi^0 ee$ is the invariant mass of the photon pair. Obviously, it will be important for $K_L^0 \rightarrow \pi^0 ee$ experiments to achieve the best possible π^0 mass resolution. Another strategy that can be used to reduce the background from $K_L^0 \rightarrow \gamma\gamma ee$ is the use of phase-space fiducial cuts. Such cuts depend on the fact that the processes $K_L^0 \rightarrow \gamma\gamma ee$ and $K_L^0 \rightarrow \pi^0 ee$ have rather different phase-space distributions. Internal-bremsstrahlung photons tend to have low energy and they tend to be emitted in the same direction as one of the electrons. Cuts on the energy and angle of the photons can be used to reduce $K_L^0 \rightarrow \gamma\gamma ee$ relative to $K_L^0 \rightarrow \pi^0 ee$. In a sensitive $K_L^0 \rightarrow \pi^0 ee$ experiment it will be necessary to require $m_{ee} > m_{\pi^0}$ to eliminate backgrounds involving $e^+ e^-$ pairs from π^0 decay. In the absence of an $e^+ e^-$ mass cut, there is a fundamental physics background from $K_L^0 \rightarrow \pi^0 \pi^0$ followed by $\pi^0 \rightarrow ee$. If $\pi^0 \rightarrow ee$ occurs at the unitarity-limit branching ratio of 4.7×10^{-8}, then the effective background branching ratio for $K_L^0 \rightarrow \pi^0 ee$ is 8.5×10^{-11}.

The main body of this paper is divided into four sections. In Sec. II, I consider classical radiation from an $e^+ e^-$ pair. The main purpose of this section is to provide insight into the angular distribution of internal bremsstrahlung photons, including how much reduction

of the background can be expected from a photon angle cut. Sec. III describes the QED calculation of $K_L^0 \rightarrow \gamma\gamma ee$. Section IV is devoted to an examination of the effect of phase space fiducial cuts on the $K_L^0 \rightarrow \gamma\gamma ee$ background and the $K_L^0 \rightarrow \pi^0 ee$ signal. The implications of these results are discussed in Sec. V.

II. CLASSICAL RADIATION FROM AN ELECTRON-POSITRON PAIR

The following equation is the classical center-of-mass energy spectrum for internal bremsstrahlung from a pair of oppositely charged particles.[6]

$$\frac{dE}{d(\hbar\omega)d(\cos\theta)} = \frac{\alpha}{2\pi}\left[\frac{\beta^2\sin^2\theta}{(1-\beta\cos\theta)^2} + \frac{\beta^2\sin^2\theta}{(1+\beta\cos\theta)^2} + \frac{2\beta^2\sin^2\theta}{1-\beta^2\cos^2\theta}\right]. \tag{1}$$

The variable $\beta = v/c$ is the final velocity of the two particles and α is the fine-structure constant. The first and second terms are the direct terms for radiation from the two particles. The third term is the interference term, which is constructive and nearly isotropic for relativistic particles. It is instructive to change variables from the polar angle θ to rapidity η ($\tanh\eta = \cos\theta$). The result of this substitution is

$$\frac{dE}{d(\hbar\omega)d\eta} = \frac{2\alpha}{\pi}\frac{\gamma^4\beta^2}{(\gamma^2 + \sinh^2\eta)^2}, \tag{2}$$

where $\gamma = (1-\beta^2)^{-1/2}$. Integrating the intensity spectrum over θ or η gives the result[7]

$$\frac{dE}{d(\hbar\omega)} = \frac{2\alpha}{\pi}\left[\left|\frac{1+\beta^2}{\beta}\right|\text{arccosh}\gamma - 1\right]. \tag{3}$$

Equation (2) represents a rapidity plateau of height $2\alpha\beta^2/\pi$ with a full width [Eq. (3) divided by $2\alpha\beta^2/\pi$]

$$W = \left|\frac{1+\beta^2}{\beta^3}\right|\text{arccosh}\gamma - \frac{1}{\beta^2}. \tag{4}$$

In $K_L^0 \rightarrow \pi^0 ee$ experiments, one encounters $e^+ e^-$ pairs with masses from m_{π^0} to $m_{K_0} - m_{\pi^0}$. For these pair masses, the width of the rapidity plateau varies from 10.2
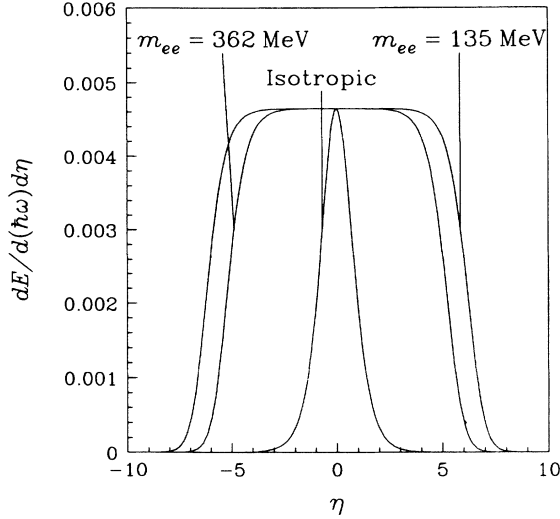
FIG. 1. Rapidity spectra for classical radiation from an e^+e^- pair in the pair center of mass.

FIG. 2. Feynman diagrams for (a) $K_L^0 \to \gamma ee$ and (b)–(e) $K_L^0 \to \gamma\gamma ee$.

to 12.1 (see Fig. 1). For comparison, the width (area divided by height) of an isotropic distribution $(dE/d\eta \propto \operatorname{sech}^2\eta)$ is 2. In other words, classically, from 19.7% to 16.5% of the internal-bremsstrahlung radiation is emitted isotropically in the e^+e^- pair center of mass. If the π^0 is at rest in the e^+e^- pair center of mass, which is the case when the pair mass has its maximum value, a photon angle cut can reduce $K_L^0 \to \gamma\gamma ee$ relative to $K_L^0 \to \pi^0 ee$ by no more than a factor of 6. For pair masses below the maximum, the motion of the π^0 causes an anisotropy in the angular distribution of signal photons, which may allow a (slightly) more effective photon angle cut.

III. QUANTUM-ELECTRODYNAMIC CALCULATION OF $K_L^0 \to \gamma\gamma ee$

The main contribution to the process $K_L^0 \to \gamma ee$ comes from the Feynman diagram shown in Fig. 2(a). The differential decay spectrum for $K_L^0 \to \gamma ee$ is given by the equation[8]

$$\Gamma_{\gamma\gamma}^{-1}\frac{d\Gamma}{dx} = \frac{2\alpha}{3\pi}\frac{(1-x)^3}{x}\left[1+\frac{2m_e^2}{xm_{K^0}^2}\right]$$
$$\times \left[1-\frac{4m_e^2}{xm_{K^0}^2}\right]^{1/2}|f(x)|^2 , \tag{5}$$

where $x = m_{ee}^2/m_{K^0}^2$ and $f(x)$ is a form factor that parametrizes the dynamics of the K_L^0-γ-γ vertex and $f(0)=1$. Theoretical predictions for $K_L^0 \to \gamma ee$ and $K_L^0 \to \gamma\gamma ee$ are normalized using the measured branching ratio for $K_L^0 \to \gamma\gamma$. I use the particle data group[9] value of $(5.70\pm0.23)\times10^{-4}$. If one assumes that $f(x)=1$ for all x, then the branching ratio for $K_L^0 \to \gamma ee$ is predicted to be 9.1×10^{-6}. The form factor $f(x)$ also appears in the
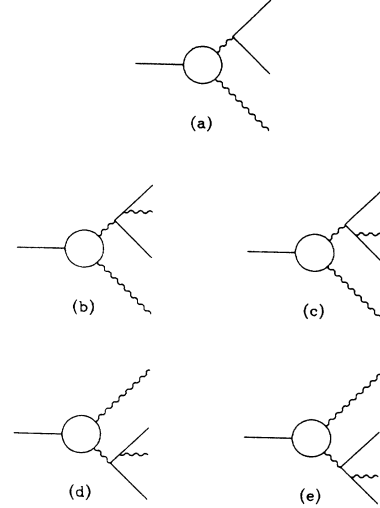
matrix element for $K_L^0 \to \gamma\gamma ee$. I use the form-factor parametrization of Bergström, Massó, and Singer:[10]

$$f(x) = \frac{1}{1-0.418x}$$
$$+ \frac{C\alpha_{K^*}}{1-0.311x}\left[\frac{4}{3}-\frac{1}{1-0.418x}-\frac{1}{9(1-0.405x)}\right.$$
$$\left. - \frac{2}{9(1-0.238x)}\right] . \tag{6}$$

This form assumes vector-meson dominance of the photon coupling. The first term represents the coupling of ρ, ω, and ϕ to the pseudoscalars π^0, η, and η'. The second term represents the coupling of ρ, ω, and ϕ to K^*. The second term vanishes for on-shell photons $(x=0)$. C is a dimensionless combination of known coupling constants[11] with the value $C=2.5$. The dimensionless parameter α_{K^*} characterizes the strength of the vector-vector weak interaction relative to the pseudoscalar-pseudoscalar interaction. I use the value[12] $\alpha_{K^*}=-0.28$.

There are four Feynman diagrams for the process $K_L^0 \to \gamma ee$ with an internal bremsstrahlung [Fig. 2(b)–2(e)]. The full matrix element corresponding to these Feynman diagrams has been calculated in order to calculate radiative corrections to the decay $\pi^0 \to \gamma ee$.[13,14]

TABLE I. Predicted branching ratio of $K_L^0 \to \gamma\gamma ee$ for various infrared cutoffs.

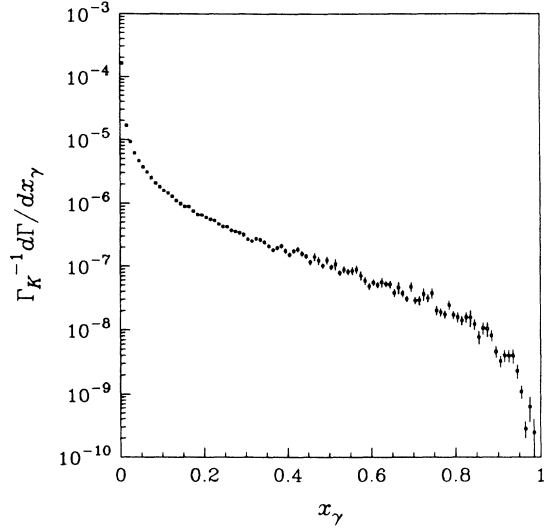| Infrared cutoff (MeV)	$B(K_L^0 \to \gamma\gamma ee)$	$B(K_L^0 \to \gamma\gamma ee)/B(K_L^0 \to \gamma ee)$ (%)
$E_\gamma > 5$	5.8×10^{-7}	6.1
$E_\gamma > 10$	4.2×10^{-7}	4.4
$E_\gamma > 15$	3.3×10^{-7}	3.4
$\lvert m_{\gamma\gamma}-m_{\pi^0}\rvert < 5$	2.8×10^{-8}	0.29

FIG. 3. Two-photon invariant-mass spectrum for $K_L^0 \rightarrow \gamma\gamma ee$.

The QED results quoted in this paper are based on the computer program described in Ref. 14.

As is the case for all bremsstrahlung processes, $K_L^0 \rightarrow \gamma\gamma ee$ is infrared divergent. The branching ratio for $K_L^0 \rightarrow \gamma\gamma ee$ depends on the infrared cutoff. Table I shows the branching ratio for $K_L^0 \rightarrow \gamma\gamma ee$ for several different infrared cutoffs. In $K_L^0 \rightarrow \pi^0 ee$ experiments, the infrared cutoff comes from the requirement that the photon pair have a mass close to the π^0 mass. Figure 3 shows the photon pair mass differential decay spectrum, $\Gamma_{\gamma\gamma}^{-1} d\Gamma /dx$, where $x_\gamma = m_{\gamma\gamma}^2 /m_{K^0}^2$. The effective branching ratio for the $K_L^0 \rightarrow \gamma\gamma ee$ background depends linearly on the experimental π^0 mass resolution. In this paper, I assume a π^0 mass cut of ± 5 MeV, which gives a branching ratio for $K_L^0 \rightarrow \gamma\gamma ee$ of 2.8×10^{-8}. As yet, no e^+e^- mass cut has been imposed. The requirement that $m_{ee} > m_{\pi^0}$ eliminates 81% of the remaining $K_L^0 \rightarrow \gamma\gamma ee$ background, but only 21% of the phase space for $K_L^0 \rightarrow \pi^0 ee$, for an effective background branching ratio of $(2.8 \times 10^{-8})(0.19)/(0.79) = 6.7 \times 10^{-9}$. For a vector matrix element (see the following section), the fraction of $K_L^0 \rightarrow \pi^0 ee$ events eliminated by the e^+e^- mass cut is 35%. In this case the effective background branching ratio becomes 8.1×10^{-9}.

IV. PHASE-SPACE FIDUCIAL CUTS

Further reductions in the $K_L^0 \rightarrow \gamma\gamma ee$ background require the use of additional phase-space fiducial cuts. Any phase-space fiducial cut can be characterized by its efficiencies for signal and background events, $\epsilon_{\pi^0 ee}$ and $\epsilon_{\gamma\gamma ee}$. The branching ratio sensitivity at which one expects one background event depends on the ratio of the background and signal efficiencies:

$$B = 8.1 \times 10^{-9} \frac{\epsilon_{\gamma\gamma ee}}{\epsilon_{\pi^0 ee}} . \tag{7}$$

The constant appearing in the above equation assumes a

vector matrix element for $K_L^0 \rightarrow \pi^0 ee$. An ideal phase-space cut would have $\epsilon_{\gamma\gamma ee} \ll \epsilon_{\pi^0 ee} \sim 1$. The extent to which this ideal can be achieved is the subject of this section.

The phase space for $K_L^0 \rightarrow \gamma\gamma ee$ has five dimensions if the photon pair mass is allowed to vary. I parametrize four-body phase space in terms of the following five variables, where p_1 and p_2 are the four-momenta of the electron and positron, respectively, k_1 and k_2 are the four-momenta of the two photons and P is the four-momentum of the parent kaon:

$$x = \frac{(p_1 + p_2)^2}{m_{K^0}^2} , \tag{8}$$

$$x_\gamma = \frac{(k_1 + k_2)^2}{m_{K^0}^2} , \tag{9}$$

$$y = \frac{2P \cdot (p_1 - p_2)}{m_{K^0}^2 \lambda^{1/2}(1, x, x_\gamma)} , \tag{10}$$

$$y_\gamma = \frac{2P \cdot (k_1 - k_2)}{m_{K^0}^2 \lambda^{1/2}(1, x, x_\gamma)} , \tag{11}$$

ϕ = angle between $\mathbf{p}_1 \times \mathbf{p}_2$ and $\mathbf{k}_1 \times \mathbf{k}_2$

in the center of mass ,   (12)

where $\lambda(a, b, c) = a^2 + b^2 + c^2 - 2(ab + bc + ac)$. The $K_L^0 \rightarrow \pi^0 ee$ Dalitz plot is parametrized by x and y. The variables y_γ and ϕ are the decay angles of the photon pair in the photon pair center of mass ($y_\gamma = \cos\theta^*$ and $\phi = \phi^*$) relative to axes defined by the e^+e^- pair ($z \| \mathbf{p}_1 + \mathbf{p}_2$, $x \perp$ to z in the direction of $\mathbf{p}_1 - \mathbf{p}_2$). In terms of these variables, the three- and four-body differential decay spectra are related to the square of the invariant matrix element as follows:

$$\frac{d\Gamma}{dx \, dy} = \frac{m_{K^0}}{64(2\pi)^3} \lambda^{1/2}(1, x, x_{\pi^0}) |\mathcal{M}|^2 , \tag{13}$$

$$\frac{d\Gamma}{dx \, dy \, dx_\gamma dy_\gamma d\phi} = \frac{m_{K^0}^3}{1024(2\pi)^6} \lambda^{1/2}(1, x, x_\gamma) |\mathcal{M}|^2 , \tag{14}$$

where $x_{\pi^0} = m_{\pi^0}^2 /m_{K^0}^2$. Equation (14) includes a statistical factor of $\frac{1}{2}$ because there are two identical photons in the final state. Considered as a four-body decay, $K_L^0 \rightarrow \pi^0 ee$ has a δ-function distribution in x_γ at $x_\gamma = x_{\pi^0}$ and a flat distribution in y_γ and ϕ. The limits of phase space are defined by the conditions

$$x > \frac{4m_e^2}{m_{K^0}^2} , \tag{15}$$

$$x_\gamma > 0 , \tag{16}$$

$$\lambda(1, x, x_\gamma) > 0 , \tag{17}$$

$$|y| < \beta , \tag{18}$$

$$|y_\gamma| < 1 , \tag{19}$$

$$0 < \phi < 2\pi , \tag{20}$$

where

$$\beta = \left[1 - \frac{4m_e^2}{x m_{K^0}^2} \right]^{1/2} . \qquad (21)$$

A. Dalitz plot for $K_L^0 \to \pi^0 ee$

A quantitative evaluation of Eq. (7) requires a model for the process $K_L^0 \to \pi^0 ee$. In this paper, I assume a vector interaction (single-photon) model. In this model, the differential decay spectrum is given by the equation[1]

$$\frac{d\Gamma}{dx\, dy} = \frac{\alpha^2 G_8^2 m_{K^0}^5}{16\pi} \lambda^{3/2}(1, x, x_{\pi^0})(1 - y^2)|\phi(x)|^2 , \qquad (22)$$

where G_8 is a coupling constant and $\phi(x)$ is a form factor [I assume that $\phi(x) =$ constant]. The general features of the decay spectrum can be understood in terms of conservation of angular momentum. The quantum numbers of the e^+e^- pair are $J^{PC} = 1^{--}$. In order to conserve angular momentum, the e^+e^- pair must be longitudinally polarized and it must be moving in a p wave relative to the π^0. The longitudinal polarization of the e^+e^- pair causes a decay angular distribution in the e^+e^- center of mass of $\sin^2\theta$. This accounts for the factor $1 - y^2$ ($y \approx \cos\theta$). Another feature of the decay spectrum is that it falls in x faster than phase space by a factor of $\lambda(1, x, x_{\pi^0}) = 4|\mathbf{p}_1 + \mathbf{p}_2|^2/m_{K^0}^2 = 4|\mathbf{p}_{\pi^0}|^2/m_{K^0}^2$. This behavior is due to an orbital angular momentum barrier. As the e^+e^- pair mass increases toward the kinematic limit, the total momentum of the e^+e^- pair relative to the π^0 goes to zero. In order to have one unit of orbital angular momentum, the impact parameter of the e^+e^- pair relative to the π^0 must increase, becoming infinite at the kinematic limit.

B. Dalitz-plot cuts

Figure 4 shows the e^+e^- pair mass spectrum, $d\Gamma/dx$, for $K_L^0 \to \gamma\gamma ee$ and $K_L^0 \to \pi^0 ee$ for both a vector matrix element [Eq. (22)] and phase space [Eq. (13)]. Both $\pi^0 ee$ spectra have been arbitrarily normalized to a branching ratio of 10^{-9}. It is clear from Fig. 4 that no e^+e^- pair mass cut (by itself) can reduce the background to a level anywhere near 10^{-11}. Indeed, above the π^0 mass, the vector e^+e^- pair mass spectrum falls almost as rapidly as the background e^+e^- pair mass spectrum. An analysis of the detailed shapes of the vector $\pi^0 ee$ and $\gamma\gamma ee$ x distributions reveals that a cut on the invariant mass of the e^+e^- pair can reduce the background relative to the signal by less than a factor of 2. A cut on m_{ee} would be more effective in the case of phase space or a scalar matrix element (but see the section on photon cuts below).

One might also consider a cut on the other Dalitz-plot variable y. As noted above, the $1 - y^2$ distribution of the vector matrix element for $K_L^0 \to \pi^0 ee$ corresponds to the longitudinal polarization of the e^+e^- pair. On the other hand, the y distribution for $K_L^0 \to \gamma\gamma ee$ is close to the y distribution of a transversely polarized vector, namely,
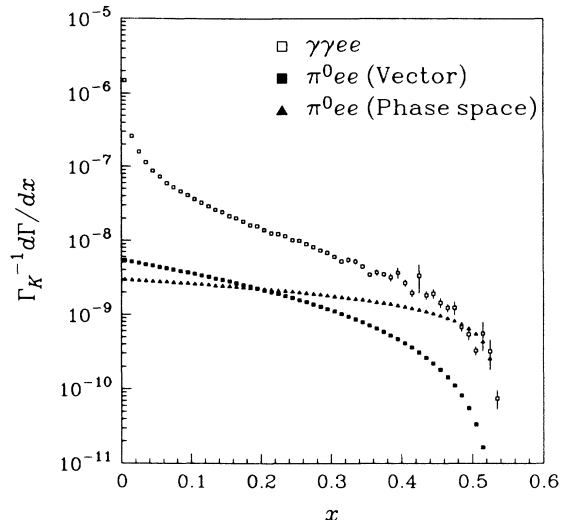

FIG. 4. Electron-positron invariant-mass spectra for $K_L^0 \to \gamma\gamma ee$ and $K_L^0 \to \pi^0 ee$.

$1 + y^2$. Given these two distributions, the maximum reduction of background relative to the signal from a cut on y is a factor of 2.

C. Photon cuts

Given the ineffectiveness of Dalitz-plot cuts in reducing $K_L^0 \to \gamma\gamma ee$ relative to $K_L^0 \to \pi^0 ee$, the main weapons in reducing the background will have to be cuts on the angles and energies of the photons, or, in other words, on y_γ and ϕ. Bremsstrahlung photons tend to have low energy and they tend to be emitted in the same direction as one of the two electrons. The tendency for bremsstrahlung photons to have low energy is measured directly by the phase-space variables y_γ. $K_L^0 \to \gamma\gamma ee$ events will have a y_γ distribution heavily skewed toward $y_\gamma = \pm 1$, whereas $K_L^0 \to \pi^0 ee$ events must have a flat y_γ distribution.
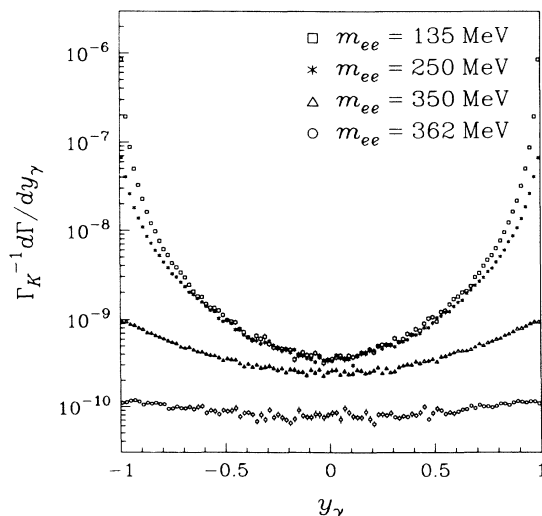
Figure 5 shows the differential decay spectrum

FIG. 5. Two-photon energy-asymmetry spectra for $K_L^0 \to \gamma\gamma ee$.

$d\Gamma/dy_\gamma$ for several e^+e^- pair masses. As the e^+e^- mass increases, the y_γ distribution becomes progressively flatter. This behavior follows from energy and momentum conservation. When $m_{ee} = m_{\pi^0}$, photon energies in the center of mass can vary over the fairly wide range from 20 to 229 MeV. As the e^+e^- pair mass increases, the allowed range of photon energies becomes narrower. At the kinematic limit, both photons are required to have

exactly 67.5 MeV of energy (i.e., half of the π^0 mass). A cut on y_γ, which is quite effective at low e^+e^- pair masses, becomes progressively less effective for larger e^+e^- pair masses.

The rapidity of the two photons in the e^+e^- center of mass is given in terms of the five phase-space variables by the following
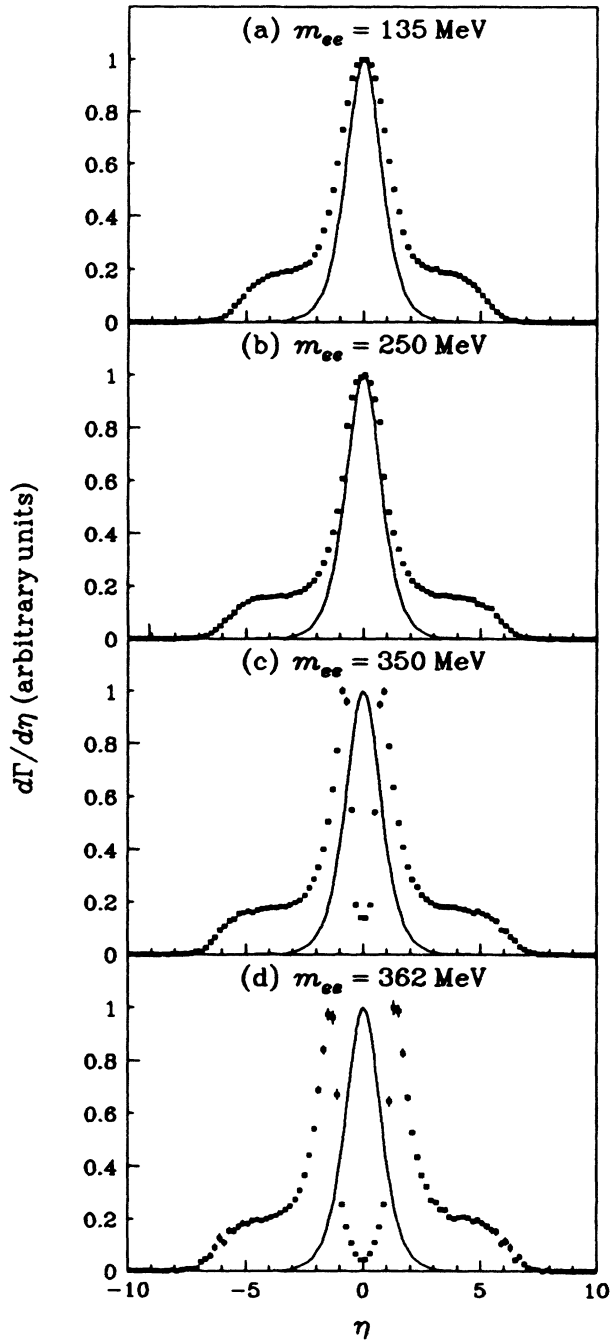

FIG. 6. Photon rapidity spectra for $K_L^0 \to \gamma\gamma ee$ in the e^+e^- center of mass. The solid line corresponds to an isotropic distribution.

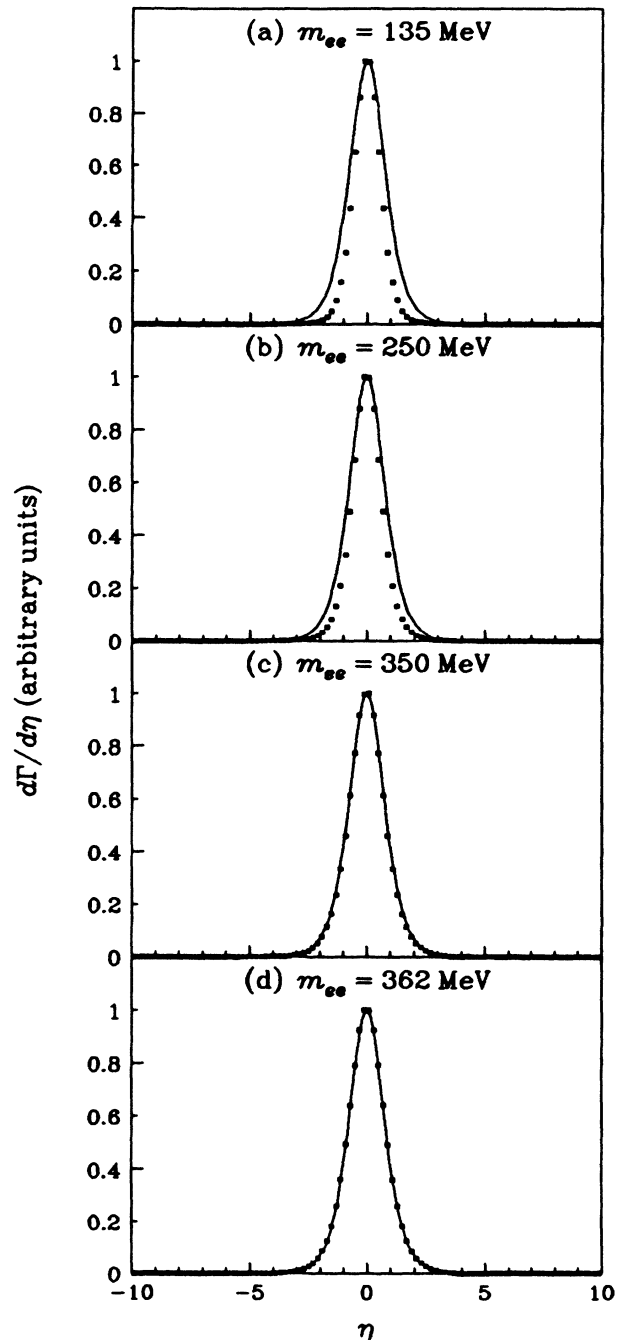FIG. 7. Photon rapidity spectra for $K_L^0 \to \pi^0 ee$ ($\pi^0 \to \gamma\gamma$) in the e^+e^- center of mass. The solid line corresponds to an isotropic distribution.

$$\tanh\eta_{1,2} = \frac{y\lambda^{1/2}(1,x,x_\gamma)\pm yy_\gamma(1-x-x_\gamma)\mp 2[xx_\gamma(\beta^2-y^2)(1-y_\gamma^2)]^{1/2}\cos\phi}{\beta[1-x-x_\gamma\pm y_\gamma\lambda^{1/2}(1,x,x_\gamma)]} , \qquad (23)$$

where β is given by Eq. (21). The upper and lower signs in Eq. (23) are for photons 1 and 2, respectively. Figure 6 shows photon rapidity distributions for several e^+e^- pair masses for the process $K_L^0 \rightarrow \gamma\gamma ee$. At lower e^+e^- pair masses, we can interpret the photon rapidity distribution as the superposition of a central peak (for the direct photon) and a classical rapidity plateau (for the bremsstrahlung photon). At higher pair masses, reduced phase space causes the angles of the two photons to become correlated. Figure 7 shows photon rapidity distributions for $K_L^0 \rightarrow \pi^0 ee$. At low e^+e^- pair masses, the photon rapidity distribution is narrower than an isotropic distribution because of the $1-y^2$ dependence of the Dalitz plot. At high e^+e^- pair masses, the photon rapidity distribution becomes isotropic due to the π^0 being at rest in the e^+e^- center of mass. A comparison of Figs. 6 and 7 shows that a cut on photon angle (rapidity) retains its effectiveness at high e^+e^- pair masses and even becomes more effective. However, this is not enough to compensate for the opposite trend in the y_γ cut.

We can conclude that the $K_L^0 \rightarrow \gamma\gamma ee$ background is most tractable for e^+e^- pair masses just above the π^0 mass. The vector model for $K_L^0 \rightarrow \pi^0 ee$, with its falling x distribution and favorable y distribution is actually one of the better ones in terms of background. In particular, it is better than pure phase space.

D. The best possible phase-space cut

Every point in $\pi^0 ee$ phase space can be characterized by the ratio R of the differential decay spectrum for $K_L^0 \rightarrow \pi^0 ee$ to the decay spectrum for $K_L^0 \rightarrow \gamma\gamma ee$:

$$R(x,y,y_\gamma,\phi) = \frac{d\Gamma^{\pi^0 ee}}{dx\,dy\,dy_\gamma\,d\phi} \Big/ \frac{d\Gamma^{\gamma\gamma ee}}{dx\,dy\,dy_\gamma\,d\phi} , \qquad (24)$$

$$= \frac{\dfrac{d\Gamma^{\pi^0 ee}}{dx\,dy\,dy_\gamma\,d\phi}}{\displaystyle\int_{x_{\gamma\min}}^{x_{\gamma\max}} \dfrac{d\Gamma^{\gamma\gamma ee}}{dx\,dy\,dx_\gamma\,dy_\gamma\,d\phi}\,dx_\gamma} , \qquad (25)$$

$$\approx \frac{\dfrac{d\Gamma^{\pi^0 ee}}{dx\,dy}}{16\pi x_{\pi^0}\left|\dfrac{\Delta m}{m_{\pi^0}}\right|\dfrac{d\Gamma^{\gamma\gamma ee}}{dx\,dy\,dx_\gamma\,dy_\gamma\,d\phi}\Big|_{x_\gamma = x_{\pi^0}}} , \qquad (26)$$

where $\Delta m = 5$ MeV is the π^0 mass cut. The best possible phase-space cut (for a given set of model assumptions) is the requirement $R > R_{\min}$. This cut is optimal in the sense that for a given signal efficiency ($\epsilon_{\pi^0 ee}$), the background efficiency ($\epsilon_{\gamma\gamma ee}$) and hence the effective background branching ratio [Eq. (7)] are made as small as possible.

One of the model assumptions that goes into the definition of R is the overall normalization of the $K_L^0 \rightarrow \pi^0 ee$ spectrum. For the numerical results quoted below, the normalization was fixed by arbitrarily assuming a branching ratio for $K_L^0 \rightarrow \pi^0 ee$ of 10^{-9} (as in Fig. 4). Numerical results that do not explicitly involve R (such as efficiencies and branching ratios) are independent of the choice of normalization. The value 10^{-9} for the branching ratio of $K_L^0 \rightarrow \pi^0 ee$ has been chosen for convenience in comparing $\pi^0 ee$ and $\gamma\gamma ee$ spectra (i.e., so that the former are not too small compared to the latter).

R is just another way of labeling phase space. R can be regarded as a phase-space variable on an equal footing with the other phase-space variables. Figure 8 shows the differential decay spectrum $d\Gamma/d(\log_{10}R)$ for $K_L^0 \rightarrow \gamma\gamma ee$ and for vector $K_L^0 \rightarrow \pi^0 ee$. Figure 8 contains enough information to calculate $\epsilon_{\pi^0 ee}$ and $\epsilon_{\gamma\gamma ee}$ for any value of $R_{\min}$. The result of this calculation is shown in Fig. 9, which shows $\epsilon_{\pi^0 ee}$ and $\epsilon_{\gamma\gamma ee}$ as a function of $R_{\min}$. Figure 10 shows the effective background branching ratio [Eq. (7)] as a function of $R_{\min}$. Finally data from Figs. 9 and 10 have been combined to give the background branching ratio as a function of $\epsilon_{\pi^0 ee}$ (Fig. 11).

The tightest possible phase cut is one that eliminates all of phase space except for one point. The point where R achieves its largest value has the following phase-space coordinates: $x=x_{\pi^0}$, $y=y_\gamma=0$, and $\phi=\pi/2$ or $3\pi/2$. Based on the discussions of Sec. IV, parts B and C, this is exactly the point in phase space that one would expect to have the best signal-to-background ratio. The value $x=x_{\pi^0}$ corresponds to $m_{ee}=m_{\pi^0}$, which is the minimum
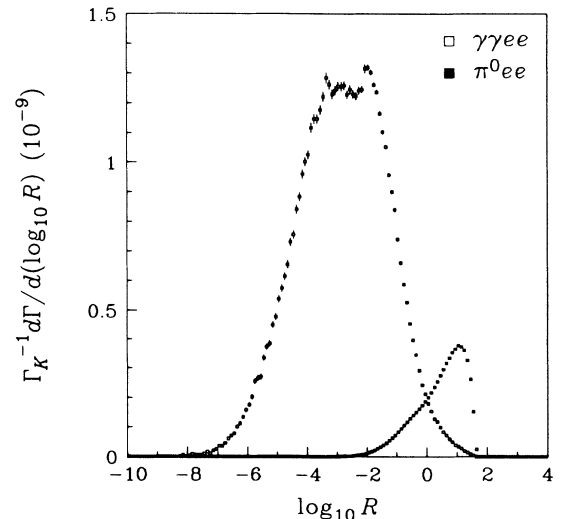

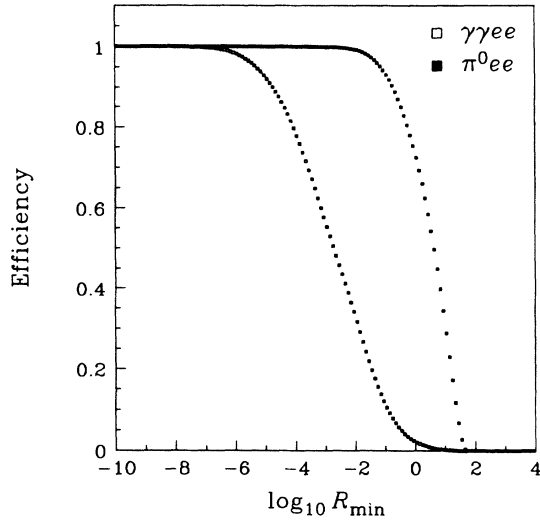FIG. 8. $\log_{10}R$ spectra for $K_L^0 \rightarrow \gamma\gamma ee$ and $K_L^0 \rightarrow \pi^0 ee$.

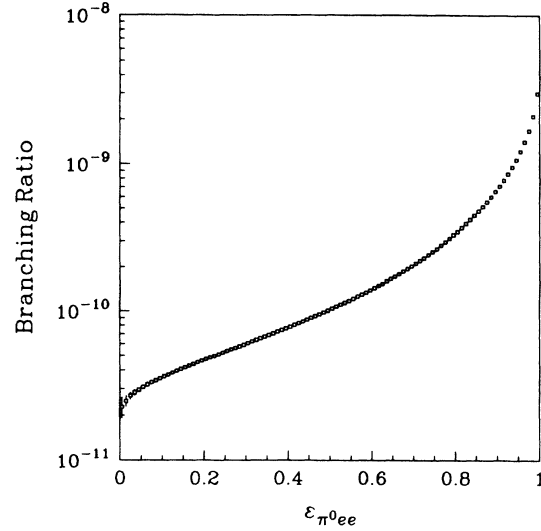FIG. 9. Efficiency of R cut as a function of R_{min} for $K_L^0 \to \gamma\gamma ee$ and $K_L^0 \to \pi^0 ee$.

FIG. 11. Background branching ratio as a function of the efficiency of the R cut for $K_L^0 \to \pi^0 ee$.

e^+e^- pair mass allowed by the phase-space fiducial cut $m_{ee} > m_{\pi^0}$. The value $y = 0$ is the point at which the $\pi^0 ee$ y distribution $(1-y^2)$ is maximized relative to the $\gamma\gamma ee$ y distribution $(1+y^2)$. Finally, the bremsstrahlung photon has the largest possible energy and angle at $y_\gamma = 0$ and $\phi = \pi/2$ or $3\pi/2$.

The value of R at this point in phase space is 47.5. If just this one phase-space point is accepted, the effective background branching ratio is $B = 10^{-9}/47.5 = 2.2 \times 10^{-11}$. Note that this branching ratio is the same as the end points of the curves in Figs. 10 and 11. Given the model assumptions of this paper, this is the lowest $\gamma\gamma ee$ background that can be achieved by any $K_L^0 \to \pi^0 ee$ experiment.

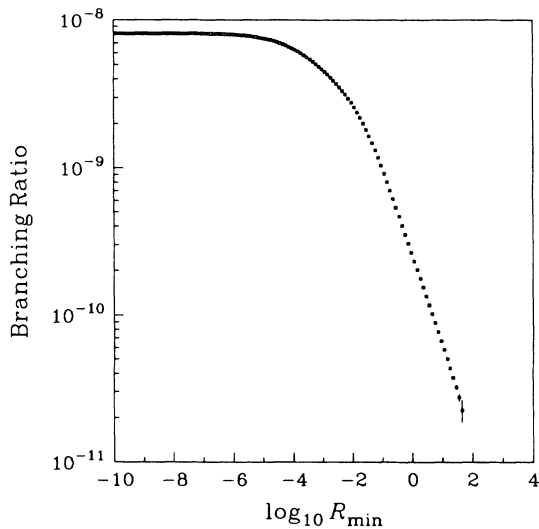FIG. 10. Background branching ratio as a function of R_{min}.

V. DISCUSSION

The process $K_L^0 \to \gamma\gamma ee$ is a serious background for sensitive $K_L^0 \to \pi^0 ee$ experiments. How serious it is for a given experiment depends on the details of the experiment. The calculations in this paper do not take into account the effect of limited detector acceptance. That is, they make the unrealistic assumption of 100% acceptance. The effect of limited acceptance could well be beneficial in the sense that the acceptance for $K_L^0 \to \pi^0 ee$ could be larger than the acceptance for $K_L^0 \to \gamma\gamma ee$. However, the phase space cut represented by detector acceptance cannot be more effective in reducing background than the R cut described above. Therefore Fig. 11 represents a lower limit on the background for an experiment with acceptance $\epsilon_{\pi^0 ee}$. There will always be a brick wall at the end point of the R spectrum.

To reach a background level comparable to the standard-model prediction for $K_L^0 \to \pi^0 ee$, it is likely that future experiments will have to artificially reduce their acceptance by the use of phase-space cuts. This will compromise other aspects of these experiments. In order to achieve the same sensitivity per unit time, it will be necessary to run with larger instantaneous K_L^0 fluxes than would otherwise have been the case. This will have various negative consequences, one of which will be to exacerbate the already serious problem of accidental coincidence backgrounds. In practice, the feasibility of a tight phase-space cut will be determined by trade offs between the $K_L^0 \to \gamma\gamma ee$ background and other factors such as accidental backgrounds and flux limits.[15]

The one possibility for an open-ended reduction in the $K_L^0 \to \gamma\gamma ee$ background is an improvement in π^0 mass resolution. My assumption of a 5-MeV mass cut is roughly consistent with conventional photon-detection technology (i.e., lead-glass calorimetry) at high energy.

New materials, such as barium fluoride, may be able to improve this parameter somewhat.

The calculations in this paper depend on various physics assumptions, such as the K_L^0 electromagnetic form factor $f(x)$, and the Dalitz plot for $K_L^0 \to \pi^0 ee$. We can get some insight into the importance of the form factor as follows. The invariant mass of the virtual photon at the end point of the R spectrum is $m_{\gamma^*} = m_{K^0}/\sqrt{2}$. The square of the form factor at this mass is 2.3 ± 0.3, where the error comes from the experimental error in the parameter α_{K^*}.[12] That is, the limiting background branching ratio is 2.3 times larger than it would be with a constant form factor. For most of phase space the square of the form factor is smaller than this.

The Dalitz plot for $K_L^0 \to \pi^0 ee$ is unknown. A change in the shape of the Dalitz plot (at a given branching ratio) would not make a huge difference. It would of course be helpful if $K_L^0 \to \pi^0 ee$ occurred at a larger than expected branching ratio.

If $K_L^0 \to \pi^0 ee$ occurs at about the predicted branching ratio, then it is unlikely that there will ever be an experiment that detects this decay with negligible background from $K_L^0 \to \gamma\gamma ee$. While one can envision measuring $K_L^0 \to \pi^0 ee$ in the presence of background, this would complicate the task of untangling the various contributions to $K_L^0 \to \pi^0 ee$ (i.e., direct and indirect CP violation and the CP-conserving 2γ process).[16]

If no special steps are taken to suppress $K_L^0 \to \gamma\gamma ee$, then it should occur at a level comparable to the sensitivity of current $K_L^0 \to \pi^0 ee$ experiments. Thus it may be possible to observe the decay $K_L^0 \to \gamma\gamma ee$ and to compare these observations with predictions. This possibility has exercised the BNL E-845 Collaboration and is the subject of another paper.[17]

*Present address: Fermilab, P.O. Box 500, Batavia, IL 60510.

[1]G. Ecker, A. Pich, and E. de Rafael, Nucl. Phys. **B291**, 692 (1987).

[2]J. F. Donoghue, B. R. Holstein, and G. Valencia, Phys. Rev. D **35**, 2769 (1987); G. Ecker, A. Pich, and E. de Rafael, Nucl. Phys. **B303**, 665 (1987); C. O. Dib, I. Dunietz, and F. J. Gilman, Phys. Rev. D **39**, 2639 (1989); J. Flynn and L. Randall, Nucl. Phys. **B326**, 31 (1989).

[3]G. D. Barr et al., Phys. Lett. B **214**, 303 (1988); L. K. Gibbons et al., Phys. Rev. Lett. **61**, 2661 (1988); A. Barker et al., Phys. Rev. D **41**, 3546 (1990).

[4]K. E. Ohl et al., Phys. Rev. Lett. **64**, 2755 (1990).

[5]N. Miyake et al., brief of KEK proposal E-162, 1988 (unpublished); T. Barker et al., Fermilab proposal E-799, 1988 (unpublished); G. D. Barr et al., Letter of Interest CERN/SPSC/80-39 (unpublished).

[6]J. D. Jackson, Classical Electrodynamics, 2nd ed. (Wiley, New York, 1975), Sec. 15.6.

[7]Jackson, Classical Electrodynamics (Ref. 6), problem 15.3.

[8]N. M. Kroll and W. Wada, Phys. Rev. **98**, 1355 (1955).

[9]Particle Data Group, G. P. Yost et al., Phys. Lett. B **204**, 1 (1988).

[10]L. Bergström, E. Massó, and P. Singer, Phys. Lett. **131B**, 229 (1983).

[11]Specifically, $C = \sqrt{8\pi\alpha}\, G_{NL} f_{K^*K\gamma} m_\rho^2 / f_{K^*} f_\rho^2 f_{K\gamma\gamma}$, where α is the fine-structure constant, $G_{NL} = 1.1 \times 10^{-5}/m_\rho^2$,

$$f_{K^*K\gamma}^2 = \frac{96\pi\Gamma(K^* \to K^0\gamma)m_{K^*}^3}{(m_{K^*}^2 - m_{K^0}^2)^3},$$

$$f_\rho^2 = \frac{4\pi\alpha^2 m_\rho}{3\Gamma(\rho \to e^+e^-)}, \quad f_{K^*} = \frac{m_{K^*}}{m_\rho}f_\rho,$$

$$f_{K\gamma\gamma}^2 = \frac{64\pi\Gamma(K_L^0 \to \gamma\gamma)}{m_{K^0}^3},$$

giving $f_{K^*K\gamma} = 3.90 \times 10^{-4}$ MeV^{-1}, $f_\rho = 4.99$, $f_{K^*} = 5.78$, $f_{K\gamma\gamma} = 3.44 \times 10^{-12}$ MeV^{-1} and $C = 2.5$. Experimental values for $\Gamma(K^* \to K^0\gamma), \Gamma(\rho \to e^+e^-)$ and $\Gamma(K_L^0 \to \gamma\gamma)$ are from Ref. 9. For more information, see Ref. 10 and the references contained therein.

[12]The text value of α_{K^*} is the experimental result of the BNL E-845 Collaboration: K. E. Ohl et al., Phys. Rev. Lett. **65**, 1407 (1990); see also G. D. Barr et al., Phys. Lett. B **240**, 283 (1990).

[13]K. O. Mikaelian and J. Smith, Phys. Rev. D **5**, 1763 (1972); **5**, 2890 (1972).

[14]L. Roberts and J. Smith, Phys. Rev. D **33**, 3457 (1986).

[15]R. Coleman and B. Winstein, in Physics at Fermilab in the 1990's, edited by D. Green and H. Lubatti (World Scientific, Singapore, 1990). This document examines the feasibility of high-sensitivity $K_L^0 \to \pi^0 ee$ experiments. Various problems and challenges are considered in detail, including the problem of accidental backgrounds.

[16]See the paper by Dib et al. of Ref. 2 for an excellent discussion of the various theoretical contributions to $K_L^0 \to \pi^0 ee$.

[17]W. M. Morse et al., Yale Report No. YAUG-A-90/4, 1990 (unpublished).